AIAA JOURNAL
Vol. 33, No. 1, January 1995

Simulation of Transverse Gas Injection in Turbulent Supersonic Air Flows

F. Grasso*
University of Rome "La Sapienza," 00184 Rome, Italy
and
V. Magi†
University of Reggio Calabria, 89128 Reggio Calabria, Italy

The present paper deals with the simulation of the fluid dynamic behavior of transverse gas injection in turbulent supersonic air streams. The Favre-averaged Navier–Stokes equations are solved for a multicomponent mixture of gases. A two-equation k-ϵ turbulence model is employed that properly accounts for low Reynolds effects. The governing equations are solved by a finite volume approach with the k-ϵ model equations fully coupled with those of the mean flow, and an implicit treatment of the source terms. Several test cases are considered and the results are compared with available experimental measurements.

Nomenclature

a	= eigenvalue of inviscid flux Jacobian
$\boldsymbol{b}$	= span base vector
c	= frozen speed of sound
c_p, c_v	= constant pressure and constant volume specific heat
$c_{\epsilon_1}, c_{\epsilon_2}, c_\mu$	= turbulence model constants
D	= diffusion coefficient
d	= slot width
E	= total energy
e	= Favre-averaged internal energy
$\boldsymbol{F}$	= sum of inviscid and viscous fluxes
H	= total enthalpy
$\boldsymbol{H}$	= source term vector
h	= duct height
$\boldsymbol{K}$	= pressure derivatives
$\boldsymbol{k}$	= turbulent kinetic energy
k_B	= Boltzmann constant
M	= molecular weight; Mach number
m	= mass of molecule
$\boldsymbol{n}$	= outward unit normal
P	= turbulence production by mean velocity gradient
p	= pressure
$\boldsymbol{q}$	= total heat flux
$\boldsymbol{R}$	= right eigenvector matrix
R	= gas constant
Re_t	= turbulent Reynolds number
S	= velocity divergence; cell area
T	= temperature
u, v	= Favre-averaged velocity components
$\boldsymbol{u}_q$	= species diffusion velocity
u_τ	= friction velocity
X	= molar fraction
x, y	= x, y coordinates
Y	= mass fraction
y^+	= viscous coordinate
$\boldsymbol{W}$	= vector unknown
α	= difference of characteristic variables
β	= cell face; proportionality constant for thermal conductivity
Δs	= cell face length
δ_{ij}	= Kronecher delta
ϵ	= dissipation of turbulent kinetic energy; interaction energy parameter
λ	= thermal conductivity
μ	= viscosity
ρ	= density
$\boldsymbol{\sigma}$	= total stress tensor
σ	= turbulent Prandtl number; collision diameter
χ	= pressure derivative
Ω	= collision integral function

Superscript

ℓ	= ℓth component

Subscripts

E	= inviscid contribution
k	= turbulent kinetic energy
i, j	= cell indices
ℓ	= laminar
He	= helium
H_2	= hydrogen
num	= numerical
p, q	= pth, qth species
t	= turbulent
V	= viscous contribution
x, y	= x, y components
ϵ	= dissipation of tubulent kinetic energy
∞	= freestream

Introduction

IN the present paper we deal with the simulation of the fluid dynamic behavior of transverse gas injection in a turbulent supersonic air stream. Such a problem has already been studied by several investigators who have shown the importance of accurately predicting the complex wave pattern and separation caused by the turbulent mixing. A gaseous transverse injection at sonic conditions causes a rapid Prandtl-Meyer expansion with the formation of a Mach disk. A bow shock forms upstream of the injector as a result of the interaction between the two streams, and the flow separates due to the interaction of the bow shock with the boundary layer (as shown in Fig. 1). The importance of an accurate simulation of such phenomena stems from the fact that the successful development of

Presented as Paper 93-2925 at the AIAA 24th Fluid Dynamics Conference, Orlando, FL, July 6–9, 1993; received Nov. 22, 1993; revision received May 20, 1994; accepted for publication May 27, 1994.

*Associate Professor, Department of Mechanics and Aeronautics, Via Eudossiana, 18. Member AIAA.

†Associate Professor, Department of Fluid Mechanics and Offshore Engineering, Via E. Cuzzocrea, 48.

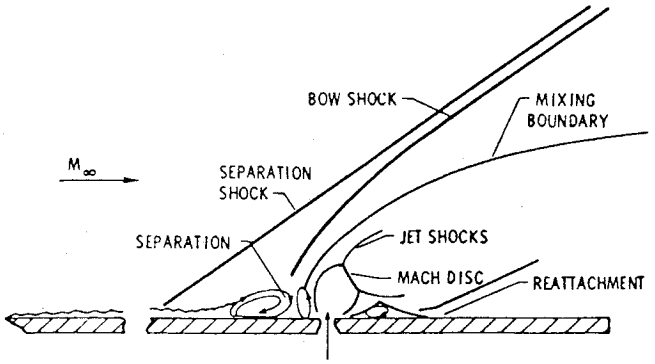

Fig. 1 Schematic of transverse gas injection flowfield, taken from Ref. 1.

scramjet propulsion systems for hypersonic cruise relies strongly on the understanding of the complexity of the flow.

This problem has been addressed by several authors[1–4] who have solved the Reynolds-averaged multicomponent Navier–Stokes equations using the Baldwin-Lomax turbulence model. Drummond and Weidner[1] and Weidner and Drummond[2] employed the explicit predictor-corrector scheme of MacCormack, and obtained a fair agreement with measured static pressure. Takahashi and Hayashi[3] applied the Harten-Yee-type explicit total variation diminishing (TVD) scheme. They have shown that some inconsistencies arise in the pressure profiles due to an overestimation of the turbulent viscosity in the proximity of the separation. Shuen and Yoon[4] analyzed the same problem by means of a high-order lower-upper symmetric successive overrelaxation scheme and obtained fair agreement with experiments.

It appears that an improved turbulence model is critical for a more accurate description of such complex fluid dynamic phenomena, in particular, the change of the flow pattern with the upstream Mach number and its effects on the mixing process. In the present work, we have solved the Favre-averaged Navier–Stokes equations for a multicomponent mixture of gases. The phenomena investigated are characterized by adverse pressure gradients and extended separation, and we employed a two-equation k-ϵ turbulence model, which satisfies the near wall asymptotic consistency.[5] The compressibility effects have been neglected due to the freestream Mach number considered in the present study. The governing equations are solved by a finite volume approach with the k-ϵ model equations fully coupled with those of the mean flow and an implicit treatment of the source terms. A high-order TVD method has been developed, which is a generalization of the Harten-Yee upwind TVD scheme[6] to multispecies turbulent gas mixtures. The model has been applied to compute transverse gas injection in supersonic air streams, and the results have been compared with available experimental measurements.

Governing Equations

The governing equations are the Favre-averaged Navier–Stokes equations for a multicomponent mixture of nonreacting thermally perfect gases that in conservation form read

$$\frac{\partial}{\partial t}\int_S \mathbf{W}\,dS + \oint_{\partial S} \mathbf{F}\cdot\mathbf{n}\,ds = 0 \tag{1}$$

The vector unknown and the sum of the inviscid and viscous fluxes are defined as follows:

$$\mathbf{W} = [\rho_q, \rho u, \rho v, \rho E]^T$$

$$\mathbf{F} = (\mathbf{F}_E - \mathbf{F}_V, \mathbf{G}_E - \mathbf{G}_V)$$

$$\mathbf{F}_E = \left[\rho_q u, \rho u^2 + p, \rho uv, \rho uH\right]^T$$

$$\mathbf{G}_E = \left[\rho_q v, \rho uv, \rho v^2 + p, \rho vH\right]^T$$

$$(\mathbf{F}_V, \mathbf{G}_V) = [-\rho_q \mathbf{u}_q, \boldsymbol{\sigma}, \mathbf{u}\cdot\boldsymbol{\sigma} - \mathbf{q}]^T$$

$$\rho = \sum\nolimits_q \rho_q$$

$$E = \sum_q Y_q e_q + u^2 + v^2/2 + k$$

$$H = E + (p/\rho)$$

The pressure is evaluated from the equation of state

$$p = T\sum_q \rho_q R_q \tag{2}$$

and the species diffusion velocity, the stress tensor, and the heat flux vector are given by

$$\rho_q \mathbf{u}_q = -\rho D_q \nabla Y_q$$

$$\boldsymbol{\sigma} = \mu\left[\nabla\mathbf{u} + (\nabla\mathbf{u})^T\right] - \tfrac{2}{3}[\mu\nabla\cdot\mathbf{u} + \rho k]\mathbf{I}$$

$$\mathbf{q} = -\lambda\nabla T + \sum_q h_q \rho_q \mathbf{u}_q$$

where μ, λ, and D_q represent the sum of the molecular and turbulent viscosity, thermal conductivity and species diffusion coefficient, respectively (with the same symbols used to indicate laminar coefficients if no confusion arises). The turbulent transport coefficients are defined by k-ϵ turbulence model that accounts for low Reynolds effects.

Thermodynamic Model

In the present work we have assumed that the gas is a multicomponent mixture of perfect gases in thermal equilibrium, and the thermodynamic relations are defined by means of a polynomial temperature curve fit. In the temperature range of interest 200 K $\le T \le$ 2000 K, the species constant pressure specific heat can be accurately represented by a second-order polynomial in temperature, whose coefficients have been determined from the JANAF thermochemical data.[7]

Molecular Diffusion Model

The molecular transport properties (viscosity, thermal conductivity, and diffusion coefficients) need to be modeled to account for the effects of temperature and composition on the transport mechanism of momentum, energy, and mass. The coefficients have been determined from a model based on the Chapman-Enskog theory which amounts to solving the Boltzmann equation for the singlet-velocity distribution function.

The following expression defining the species molecular viscosity has been used:

$$\mu_q = \frac{5}{16}\frac{(\pi m_q k_B T)^{0.5}}{\pi\sigma_q^2\Omega_\mu} \tag{3}$$

where Ω_μ is a function of the dimensionless temperature $(k_B T/\epsilon_q)$ (Ref. 8), and the mixture viscosity is found from Wilke's law[9]

$$\mu = \sum_q \frac{\mu_q}{1 + (1/X_q)\sum_{p\neq q}^{p} X_p \Phi_{q,p}} \tag{4}$$

where

$$\Phi_{q,p} = \frac{\left\{1 + [(\mu_q/\mu_p)(\rho_p/\rho_q)]^{0.5}(M_q/M_p)^{0.25}\right\}^2}{(4/\sqrt{2})[1 + (M_q/M_p)]^{0.5}} \tag{5}$$

From kinetic theory, it can be shown that the molecular diffusion of energy is proportional to that of momentum. Then, accounting for both the translational and internal structure contributions, the species thermal conductivity is

$$\lambda_q = \beta_q\left[1 + \frac{2}{3}\left(\frac{2}{5}\frac{c_{p_q}}{R_q} - 1\right)\right]c_{vq}\mu_q \tag{6}$$

and the mixture thermal conductivity is computed according to Wassiljewa's formula (see Ref. 10)

$$\lambda = \sum_q \frac{\lambda_q}{\left[1 + 1.065(1/X_q)\sum_{\substack{p \\ p\neq q}} X_p \Phi_{q,p}\right]} \tag{7}$$

The species molecular diffusion coefficient is given by

$$D_q = \frac{1 - Y_q}{\sum_{\substack{p \\ p\neq q}} X_p / D_{q,p}} \tag{8}$$

where the following expression for the binary diffusion coefficient is used:

$$D_{q,p} = 1.883\,10^{-2} \frac{\sqrt{T^3[(M_q + M_p)/M_q M_p]}}{p\sigma_{q,p}^2 \Omega_D} \tag{9}$$

and $\sigma_{q,p}$ and Ω_D are, respectively, the collision diameter of the two colliding species q-p, and the collision integral function, which are defined as[11]

$$\sigma_{q,p} = (\sigma_q + \sigma_p)/2$$

$$\Omega_D = 1.22 \cdot \bar{T}^{-0.16}$$

where $\bar{T} = T/T_{\epsilon_{q,p}}$ and $T_{\epsilon_{q,p}} = \sqrt{\epsilon_q \epsilon_p}/k_B$.

Turbulent Diffusion Model

For engineering applications, the classical high Reynolds number, k-ϵ model has been commonly used in conjunction with wall functions to simulate several wall bounded flows with some success. However, the model has its drawbacks in problems where wall transport properties are needed or in the presence of flow separation and adverse pressure gradients. To overcome these problems, a consistent asymptotic behavior in the near wall region must be enforced.[5] Moreover, for high Mach number complex flows, compressibility effects have been shown to play an important role, especially for the turbulent shock amplifying mechanism.[12] Abid et al.[13] have analyzed the incompressible flow past a backward facing step and have shown that streamwise curvature could be important in strongly recirculating flow regions. However, in the presence of shock-wave turbulent boundary-layer interactions, it is believed that curvature effects would not play a significant role with respect to the turbulence amplification mechanism induced by the shock.

In the present work a two-equation k-ϵ model of turbulence that accounts for low Reynolds effects has been used, and curvature effects have not been accounted for. Moreover, the influence of compressibility has been disregarded, since the applications is limited to supersonic Mach number flows. Following the work of Speziale et al.[5] and Grasso and Falconi[12] the k-ϵ model equations in integral vector form are

$$\frac{\partial}{\partial t}\int_S \tilde{\mathbf{W}} \mathrm{d}S + \oint_{\partial S} \tilde{\mathbf{F}} \cdot \mathbf{n}\,\mathrm{d}s = \int_S \tilde{\mathbf{H}}\,\mathrm{d}S \tag{10}$$

where

$$\tilde{\mathbf{W}} = [\rho k, \rho\epsilon]^T$$

$$\tilde{\mathbf{F}} = (\tilde{\mathbf{F}}_E - \tilde{\mathbf{F}}_V, \tilde{\mathbf{G}}_E - \tilde{\mathbf{G}}_V)$$

$$\tilde{\mathbf{H}} = [H_k, H_\epsilon]^T$$

$$\tilde{\mathbf{F}}_E = [\rho u k, \rho u \epsilon]^T$$

$$\tilde{\mathbf{G}}_E = [\rho v k, \rho v \epsilon]^T$$

$$\tilde{\mathbf{F}}_V, \tilde{\mathbf{G}}_V = \left[\left(\mu_\ell + \frac{\mu_t}{\sigma_k}\right)\nabla k, \left(\mu_\ell + \frac{\mu_t}{\sigma_\epsilon}\right)\nabla\epsilon\right]^T$$

$$\tilde{\mathbf{H}} = \begin{bmatrix} \mu_t P - \frac{2}{3}\rho k S - \rho\epsilon \\ c_{\epsilon_1}\left(\mu_t P - \frac{2}{3}\rho k S\right)\frac{\epsilon}{k} - c_{\epsilon_2} f_2 \rho \frac{\epsilon^2}{k} \end{bmatrix}$$

The turbulent viscosity μ_t is defined as

$$\mu_t = c_\mu f_\mu \rho (k^2/\epsilon) \tag{11}$$

where $c_\mu = 0.09$ and f_μ is a function of $\mathcal{O}(1/y^+)$ near the wall, and the viscous coordinate is defined as $y^+ = u_\tau y/\nu$. According to the work of Speziale et al.[5] we have used the following expressions for the wall damping functions f_2 and f_μ:

$$f_2 = [1 - \exp(-y^+/4.9)]^2$$

$$f_\mu = \left(1 + \frac{3.45}{\sqrt{Re_t}}\right)\tanh(y^+/70)$$

and, as suggested by Hanjalic and Launder,[14] the following turbulent Reynolds number $[Re_t = \rho(k^2/\mu_\ell\epsilon)]$ dependency for c_{ϵ_2} is used

$$c_{\epsilon_2} = 1.83\left[1 - (2/9)\exp\left(-Re_t^2/36\right)\right]$$

The value of the constant c_{ϵ_1} is determined according to the local equilibrium relationship.[5] Following the indications given by Grasso and Falconi,[12] we have employed a value of $\sigma_k = 1.5$, and $\sigma_\epsilon = 2$. The turbulent conductivity and species diffusion coefficients have been determined by assuming values of the turbulent Prandtl and Schimdt numbers equal to 0.9.

Numerical Solution

The solution of the governing equations for turbulent supersonic flows requires the use of robust and accurate schemes. The flux-difference splitting of Roe[15] and the flux-vector splitting of Steger and Warming[16] and Van Leer[17] have been widely used for perfect gas high-speed flow computations. Extensions of Roe's approximate Riemann solver and flux-vector splitting for real gases have been presented in Refs. 18–20.

In the present work, the k-ϵ transport equations have been fully coupled with the governing equations of the mean flow. Following the general methodology developed for the solution of high-speed flows,[19,20] we have extended a second-order TVD method to include the effects of turbulence on the transport mechanism of momentum, energy, and mass.

Space and time discretizations are separated by using the method of lines, and a system of ordinary differential equations is obtained for each computational cell. A cell-centered finite volume formulation is used, and the following discretized form of the governing equations is obtained:

$$S_{i,j}\frac{\mathrm{d}\mathbf{W}_{i,j}}{\mathrm{d}t} + \sum_{\beta=1}^{4}(\mathbf{F}_{\mathrm{num}} \cdot \mathbf{n}\Delta s)_\beta = S_{i,j}\mathbf{H}_{i,j} \tag{12}$$

where the solution vector and the source term are now

$$\mathbf{W} = [\rho_q, \rho u, \rho v, \rho E, \rho k, \rho\epsilon]^T$$

$$\mathbf{H} = [0, 0, 0, 0, H_k, H_\epsilon]^T$$

The inviscid flux discretization is based on the modified Harten-Yee method[6] generalized for a turbulent flow of a mixture of non-reacting gases. The scheme has good properties of monotonicity and conservativity in the presence of discontinuities, and it yields second-order accuracy and oscillation free solutions. By enforcing consistency at cell face $(i + \frac{1}{2}, j)$ one obtains

$$(\mathbf{F}_{E,\mathrm{num}}n_x + \mathbf{G}_{E,\mathrm{num}}n_y)_{i+\frac{1}{2},j} = \left[(\mathbf{F}_E n_x + \mathbf{G}_E n_y)_{i,j}\right.$$

$$\left. + \mathbf{F}_E n_x + \mathbf{G}_E n_y)_{i+1,j} + \mathbf{R}_{i+\frac{1}{2},j}\Phi_{i+\frac{1}{2},j}\right]/2$$

The term $\Phi_{i+1/2,j}$ is the numerical antidiffusive flux contribution that modifies the inviscid flux to make the scheme upwind biased TVD and second-order accurate. The expression of its elements $(\varphi^\ell_{i+1/2,j})$ is obtained by characteristic decomposition in the direction normal to cell face, thus obtaining

$$\varphi^\ell_{i+\frac{1}{2},j} = \tfrac{1}{2}\psi\left(a^\ell_{i+\frac{1}{2},j}\right)\left(g^\ell_{i+1,j} + g^\ell_{i,j}\right) - \psi\left(a^\ell_{i+\frac{1}{2},j} + \gamma^\ell_{i+\frac{1}{2},j}\right)\alpha^\ell_{i+\frac{1}{2},j}$$

where

$$\alpha_{i+\frac{1}{2},j} = \mathbf{R}^{-1}_{i+\frac{1}{2},j}(\mathbf{W}_{i+1,j} - \mathbf{W}_{i,j})$$

$$\gamma^{\ell}_{i+\frac{1}{2},j} = \tfrac{1}{2}\psi\left(a^{\ell}_{i+\frac{1}{2},j}\right)\left(g^{\ell}_{i+1,j} - g^{\ell}_{i,j}\right)/\alpha^{\ell}_{i+\frac{1}{2},j}$$

Here, $\psi(z)$ is Harten's entropy correction to $|z|$, and $a^{\ell}_{i+1/2,j}$ are the eigenvalues of the inviscid flux Jacobian; moreover, $\gamma^{\ell}_{i+1/2,j}$ vanishes if $\alpha^{\ell}_{i+1/2,j}$ is equal to zero. A minmod limiter has been selected for its better computational efficiency and speed of convergence

$$g^{\ell}_{i,j} = \text{minmod}\left(\alpha^{\ell}_{i+\frac{1}{2},j}, \alpha^{\ell}_{i-\frac{1}{2},j}\right)$$

where

$$\text{minmod}(x, y) = \text{sgn}(x) \cdot \max\{0, \min[|x|, y \cdot \text{sgn}(x)]\}$$

At all boundaries consistency and conservation is enforced, and the normal derivative of g is set equal to zero. To construct linearly independent eigenvectors, the base vectors are chosen in such a way as to be orthogonal to the cell face normal. Consequently, the right-eigenvector matrix of the normal inviscid flux Jacobian is

$$\mathbf{R} = \begin{bmatrix} \delta_{qr} & 0 & Y_q & Y_q & 0 \\ u & -cn_y & u + cn_x & u - cn_x & 0 \\ v & cn_x & v + cn_y & v - cn_y & 0 \\ \frac{\mathbf{u}\cdot\mathbf{u}}{2} - \frac{\chi_r}{K} & c(\mathbf{u}\cdot\mathbf{b}) & H + cu_n & H - cu_n & 0 \\ 0 & 0 & k & k & \delta_{k\epsilon} \\ 0 & 0 & \epsilon & \epsilon & \delta_{k\epsilon} \end{bmatrix}$$

and the pressure derivatives are defined as

$$K = \left(\frac{\partial p}{\partial \rho e}\right)_{\rho_q} = \frac{\sum_q \rho_q R_q}{\sum_q \rho_q c_{v,q}}$$

$$\chi_q = \left(\frac{\partial p}{\partial \rho_q}\right)_{\rho e} = R_q T - K\, e_q$$

The difference of the characteristic variables at cell face $(i + \frac{1}{2}, j)$ is given by

$$\alpha_{i+1/2,j} = \begin{bmatrix} \Delta\rho_q - \frac{\bar{Y}_q}{\bar{c}^2}\Delta p \\ \frac{\bar{\rho}}{\bar{c}}\Delta\mathbf{u}\cdot\mathbf{b} \\ \frac{1}{2}\left(\frac{\Delta p}{\bar{c}^2} + \bar{\rho}\frac{\Delta\mathbf{u}\cdot\mathbf{n}}{\bar{c}}\right) \\ \frac{1}{2}\left(\frac{\Delta p}{\bar{c}^2} - \bar{\rho}\frac{\Delta\mathbf{u}\cdot\mathbf{n}}{\bar{c}}\right) \\ \Delta(\rho k) - \frac{k}{\bar{c}^2}\Delta p \\ \Delta(\rho\epsilon) - \frac{\bar{\epsilon}}{\bar{c}^2}\Delta p \end{bmatrix}$$

where

$$\bar{(\cdot)} = (\cdot)_{i+\frac{1}{2},j}; \qquad \Delta(\cdot) = (\cdot)_{i+1,j} - (\cdot)_{i,j}$$

The values at the interfaces are calculated by using a generalization of Roe's averaging to account for the multicomponent mixture of gases with turbulent effects.

The numerical viscous fluxes are evaluated by applying Gauss theorem to a cell whose vertices are the two grid nodes at cell face $(i+\frac{1}{2}, j)$ and the centers of the two adjacent cells (i, j) and $(i+1, j)$, with a bilinear interpolation of cell-center values used to determine node values.

For turbulent flows, the system of governing equations is stiff due to the disparity between the turbulence and fluid dynamic time scales. Therefore, the time integration requires, in principle, an extremely small time step. However, for steady flows stiffness can be reduced by introducing a precondition matrix, which is related to the partial Jacobian of the source term of the turbulence model with respect to ρk and $\rho\epsilon$. The time integration of Eq. (12) is then performed by a three-stage Runge-Kutta method, where the source terms of the k and ϵ equations are treated by a point implicit algorithm.

At the inflow boundary freestream values are imposed, and k and ϵ are assigned by assuming a low value of the freestream turbulence level. For all cases, first-order extrapolation conditions have been imposed on all variables at the outflow. At the far field, depending on the flow direction, either freestream conditions are set or first-order extrapolation conditions are imposed. At the wall the no-slip condition is enforced on the velocity; the pressure is obtained by assuming a zero normal gradient and adiabatic conditions, and the normal species diffusion fluxes are set to zero. Moreover, the turbulent kinetic energy and the normal derivative of ϵ are also set equal to zero at the wall. At the gas injector, boundary conditions are specified by imposing choked conditions and setting the values of pressure and temperature obtained from the experimental test cases provided for comparisons.

Results

Transverse gas injections in supersonic air streams have been simulated to assess the influence of turbulence modeling, and the effects of the freestream Mach number on the flow structure have been studied. For all test cases the computations have been carried up to a residual decay of about four orders of magnitude with a CFL number of about 0.5–0.6, and the local time stepping approach has been employed to accelerate the convergence.

Hydrogen Injection

The first test case corresponds to hydrogen injection through a 0.02-cm slot on a flat plate. The orifce is located 25.6 cm from the leading edge of the plate, and the conditions at the injector exit are $M_{H_2} = 1.0$, $T_{H_2} = 243$ K, and $p_{H_2} = 0.728$ MPa. The flow conditions correspond to $M_\infty = 2.5$, $T_\infty = 130$ K and $p_\infty = 0.0169$ MPa. For this test case the wall pressure distribution measured by Thayer (see Ref. 1) is available. The computational domain is divided in two zones: region Ω_1 that extends between the flat plate leading edge and a section located 5 cm upstream of the slot; and region Ω_2 that extends for 10 cm centered around the orifice. The computations have been performed on a 200 × 64 mesh with normal mesh spacing ranging from $\Delta y_{\min} = 1.19 \cdot 10^{-6}$ cm to $\Delta y_{\max} = 3.0 \cdot 10^{-3}$ cm and aspect ratio varying between $AR_{\min} = 0.55$ to $AR_{\max} = 5042$. In particular, in the x direction 40 cells are distributed in Ω_1 and 160 cells in Ω_2, and approximately 30 cells are fitted within the boundary layer [with the y^+ of the near wall cells of $\mathcal{O}(0.1)$].

The iso-Mach contours are plotted in Fig. 2 which shows the flow structure under the turbulent and laminar (computed on the same grid) conditions. As already shown by Zukoski and Spaid,[21] under turbulent conditions the separated region is shorter than in the laminar case. As observed from the figure the model is able to resolve the complex pattern that arises due to the interaction of the hydrogen jet with the air stream.[21] The hydrogen expands rapidly

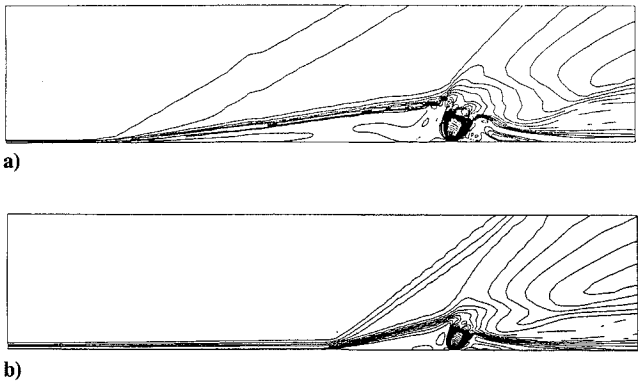

a)

b)

Fig. 2 iso-Mach line contours: a) laminar and b) turbulent.

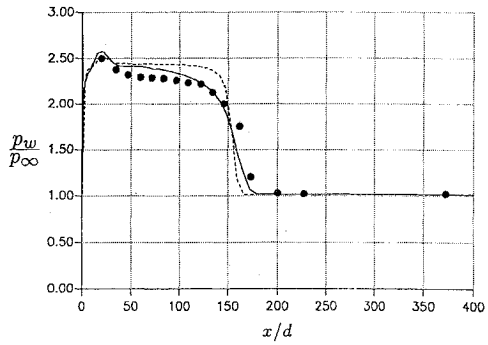

Fig. 3 Wall pressure distribution: • • •, exp. Ref. 1; ——, LR model; and - - -, BL model).

through a strong Prandtl-Meyer fan and forms a Mach disk at a distance of approximately 21 slot widths (34 in the laminar case). Two barrel shocks arise near the edges of the orifice yielding the typical budding-type shock shape.[22] The strong bow shock, which arises due to the interaction of the primary and secondary streams, is responsible for the turning of the hydrogen jet in the main flow direction. The flow separates upstream of the injector due to the interaction of the bow shock with the boundary layer (yielding a well-defined separation shock in the turbulent case and a rather weak one in the laminar case), with reattachment downstream of the orifice, and a larger separation extent in the case of laminar flow.

Figure 3 shows the wall pressure distribution vs x/d (with x measured upstream of the injector). The computed results obtained with the low Reynolds k-ϵ (LR) and Baldwin-Lomax (BL) models are compared vs the experimental data of Ref. 1. From the experiments observe that the flow separates at approximately 180 slot widths upstream of the injector (reattaching 120 slot widths downstream) with a plateau pressure level of 2.3 times the freestream pressure. The Baldwin-Lomax model predicts a separation at approximately 165 slot widths upstream of the injector and a plateau pressure value of $2.5p_\infty$. Good agreement with the experiments is observed with the LR model: the flow is predicted to separate at 179 slot widths upstream of the injector (where the separation point is here defined as the position where thte first increase in pressure is observed). The plateau pressure level is slightly overpredicted, however, the pressure rise is in good agreement with the experiments.

Figure 4 shows the pressure distribution vs y/d at 75 and 200 slot widths downstream of the injector. The figure illustrates the importance of the low Reynolds effects. Indeed, in the near wall region the LR and BL models show differences up to about 150 slot widths downstream of the injector, and those effects are confined to the recirculation region. No differences in the static pressure rise are observed, even though differences in the peak pressure associated with the bow and separation shocks are noticeable. Little effects are found in the hydrogen mass fraction distributions (not reported here) computed with LR and BL.

The sensitivity of the solution to the model constants has also been assessed by varying the values of the turbulent Prandtl numbers. The results, obtained with a different set of values $\sigma_k = 1.36$ and $\sigma_\epsilon = 1.80$, show that a reduction in the turbulent Prandtl numbers acts in the direction to decrease the turbulence dissipation, thus reducing the influence of the laminar sublayer. Consequently, the separation is delayed with a displacement of the separation point toward the injector. To assess the grid independence of the results we have also performed a computation on a coarser grid (amounting to 40 cells in the x direction in Ω_1 and 80 cells in Ω_2, and 32 cells in the y direction). The computed results, not reported here, show differences of about 10% in the separation extent and plateau pressure level.

The effects of the freestream Mach number of the primary flow have also been analyzed, and two additional simulations have been performed at $M_\infty = 3.5$ and 4.5. The computed results show that a change in the Mach number affects the upstream influence. As the Mach number increases, the jet penetration is reduced, due to the reduction of the hydrogen momentum with respect to the incoming air momentum and the separation point is displaced toward the

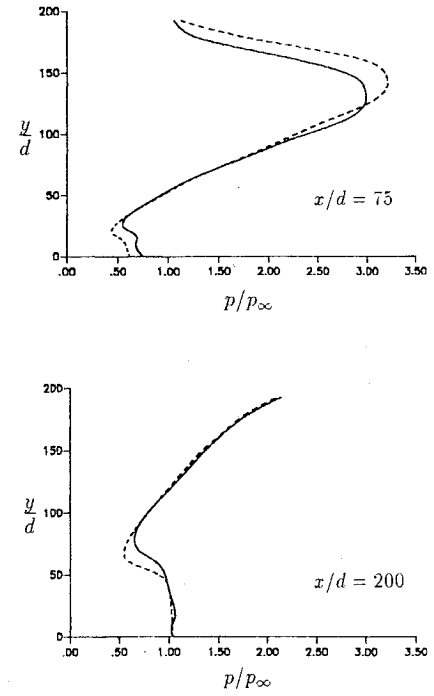

Fig. 4 Pressure distribution vs y/d at two different locations downstream of the injector: —, LR model and - - -, BL model.

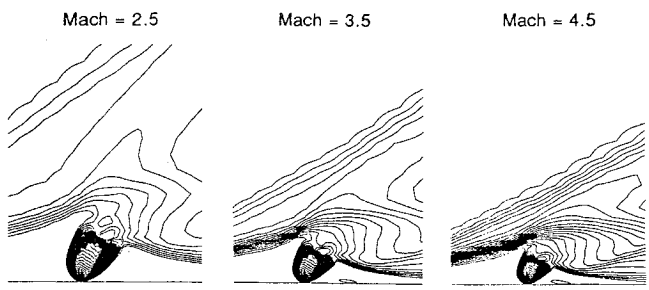

Fig. 5 iso-Mach line contours.

edge of the slot. However, the flow structure shows a geometrical similarity: the Mach disk and the upstream and downstream barrel shocks preserve the budding-type configuration.[22] Indeed, the latter is mainly determined by the choking conditions of the secondary flow rather than the primary flows, as also shown by Aso et al.[22] Those authors have studied the influence of the pressure ratio P_c/P_0 (P_c being the total pressure of the secondary flow and P_0 the total pressure of the freestream) on the upstream flow structure and have reached the same conclusions.

The details of the flow structure are presented in Fig. 5, which shows a blow up of the iso-Mach contour lines for the three Mach numbers. The wall pressure distribution vs x/d clearly shows (see Fig. 6) the influence of the Mach number on the separation extent: for $M_\infty = 3.5$ the flow separates at $x/d = 140$ and reattaches at approximately 70 slot widths downstream of the injector; for $M_\infty = 4.5$ the flow separates at $x/d = 116$ and reattaches at $x/d = -55$. The static pressure at the orifice location is plotted vs y/d in Fig. 7. The figure shows a rapid decrease in pressure due to the strong expansion of the jet, followed by a steep pressure rise through the Mach disk. Defining the jet penetration as the position at which the upstream barrel shock interacts with the Mach disk, a nearly linear variation of the jet penetration with the separation distance is obtained (as reported in Fig. 8), in agreement with experimental findings.[22] With the BL model the linear scaling is recovered only at the lower Mach numbers ($M_\infty = 2.5$ and 3.5). The reduction of the jet penetration also affects the H_2-air mixing. As the Mach number is increased, the mixing is confined to a region closer to the wall.

Finally, an additional computation has been performed at $M_\infty = 1.5$. At this Mach number the Mach disk and the (upstream

and downstream) barrel shocks change their configuration from a budding-type to a fan-type structure. Such a change can be explained as follows. The location of the oblique separation shock is influenced by the upstream Mach number, and as the Mach number is reduced the shock lifts up and moves upstream. For low-supersonic conditions, it disappears and a weak normal shock arises. As a consequence, the flow becomes subsonic ahead of the injector, thus giving rise to a fan-type configuration. This has also been observed experimentally by Aso et al.,[22] who have analyzed the effect of varying the slot width for a given upstream Mach number. The present computations show a weak normal shock standing at a distance of about $x/d = 560$, with a fan structure around the injector as shown in Fig. 9.

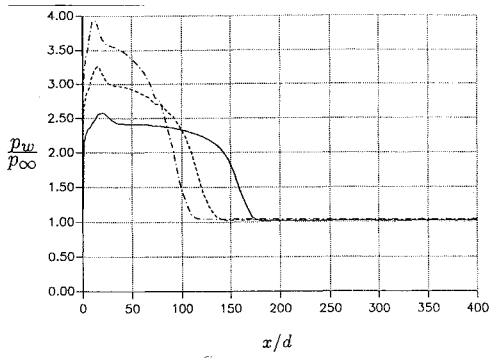

Fig. 6 Wall pressure distribution: ——, $M_\infty = 2.5$; - - -, $M_\infty = 3.5$; and - · -, $M_\infty = 4.5$.

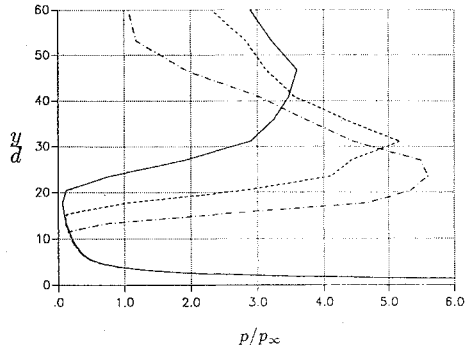

Fig. 7 Pressure distribution vs y/d at injector location: ——, $M_\infty = 2.5$; - - -, $M_\infty = 3.5$; and - · -, $M_\infty = 4.5$.

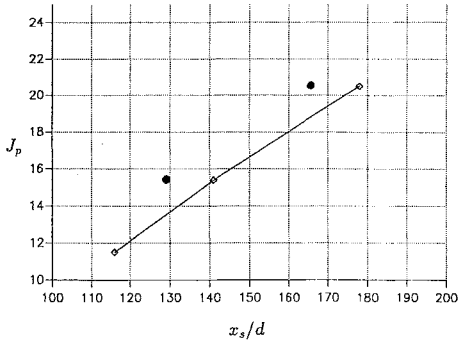

Fig. 8 Jet penetration J_p vs separation point (x_s/d): ——, LR model; and •, BL model.

Helium Injection

The second test case corresponds to helium injection from a 0.0559 cm slot in a rectangular duct 25.4 cm long and 7.62 cm high. The orifice is located 17.8 cm from the duct inlet. The air conditions at the entrance of the duct are: $M_\infty = 2.9$, $T_\infty = 108$ K and $p_\infty = 0.0663$ MPa. Helium is injected through the orifice at the following conditions: $M_{He} = 1.0$, $T_{He} = 217$ K, and $p_{He} = 1.240$ MPa. For this test case experimental results are available and they are reported in Ref. 2.

Two computations have been performed with the Baldwin-Lomax model and with the low Reynolds k-ϵ model. As in the first test case the computational domain is divided in two regions: Ω_1 that extends until a section located 7.6 cm upstream of the slot (spanned by a grid with 40 cells in x direction) and Ω_2 that is centered around the orifice and contains 160 cells in the x direction. In the transverse direction 80 cells have been used; grid stretching near the slot and in the vicinity of the lower and upper walls has been used yielding a value of y^+ of $\mathcal{O}(0.1)$ for the near wall cells. The normal mesh spacing ranges from $\Delta y_{min} = 1.46 \cdot 10^{-6}$ cm to $\Delta y_{max} = 4.74 \cdot 10^{-3}$ cm and the aspect ratio varies between $AR_{min} = 0.73$ to $AR_{max} = 2054$.

Figure 10 shows the pressure (normalized by a reference pressure equal to 2.1 MPa) distribution vs y/h at $x = 3.81$ cm downstream of the injector (approximately 68 slot widths). The results show that in the near (lower) wall region the low Reynolds model yields a better agreement with the experimental data reported in Ref. 2. Both models updperpredict the value of the pressure peak associated with the separation and bow shocks. Moreover, as already found by Weidner and Drummond,[2] both models predict separation closer to the injector, thus yielding a peak pressure closer to the lower wall.

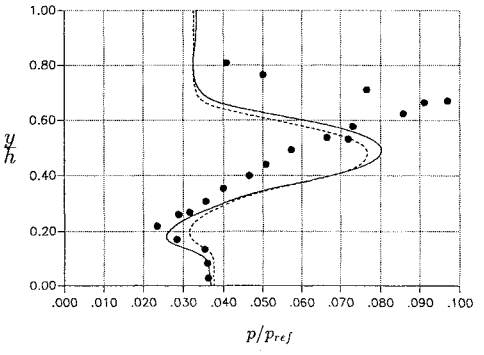

Fig. 10 Pressure distribution vs y/h at $x = 3.81$ cm: • • •, exp. Ref. 2; ——, LR model; and - - -, BL model.

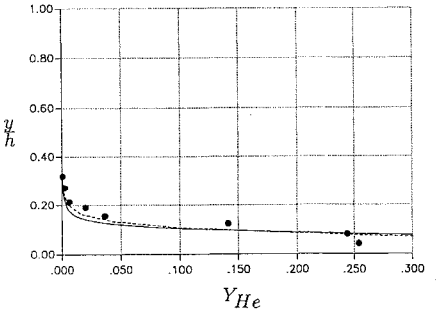

Fig. 11 Helium mass fraction distribution vs y/h at $x = 3.81$ cm: • • •, exp. Ref. 2; ——, LR model; and - - -, BL model.

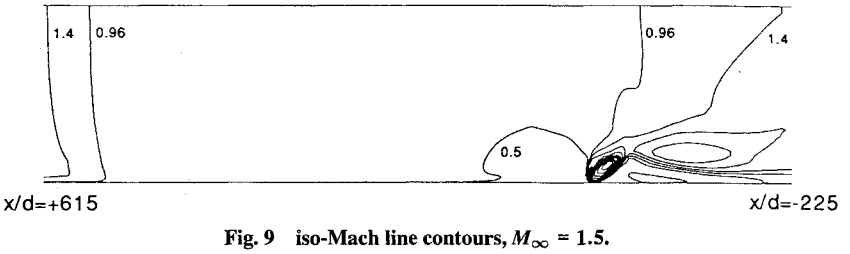

Fig. 9 iso-Mach line contours, $M_\infty = 1.5$.

The agreement between the measured and computed helium mass fraction distribution is quite satisfactory, as shown in Fig. 11.

Conclusions

In the present work, a model to simulate transverse gas injection in a turbulent supersonic air stream has been developed. The turbulence model uses a low Reynolds two-equation k-ϵ approach whose behavior has been thoroughly analyzed by comparison with the algebraic Baldwin-Lomax model and experimental results. The numerical method is based on a fully coupled strategy that uses an upwind biased second-order TVD scheme extended to a multicomponent gas mixture and includes the turbulence transport processes. The stiffness of the turbulence model equations, due to the disparity of the turbulence and fluid dynamic time scales, has been removed by a pointwise implicit treatment of the source terms.

A study of the interaction of supersonic air stream with transverse gas injected at sonic conditions shows that the detail of the complex flow pattern can be adequately represented by the low Reynolds number model. Comparisons with experimental data indicate that the model adequately resolves the interaction of the bow shock with the boundary layer, as well as the complex structure of the jet issuing from the slot. The analysis shows that the laminar sublayer plays a role in the establishment of the flow pattern. Moreover, the solution has been found to be sensitive to the model constants that affect turbulent diffusion and the production of turbulence dissipation. The model is capable of reproducing the complexity of supersonic mixing of a primary flow with a secondary (transverse) one. A geometrical similarity of the flow structure has been found for increasing freestream Mach number, giving a budding-type shock configuration. However, the budding-type structure changes to a fan-type structure as the Mach number is reduced.

Acknowledgments

This work was partly supported by Ministero dell' Università e delle Ricerca Scientifica e Tecnologica and Consiglio Nazionale delle Ricerche.

References

[1]Drummond, J. P., and Weidner, E. H., "Numerical Study of a Scramjet Engine Flowfield," *AIAA Journal,* Vol. 20, No. 9, 1982, pp. 1182–1187.

[2]Weidner, E. H., and Drummond, J. P., "Numerical Study of Staged Fuel Injection for Supersonic Combustion," *AIAA Journal,* Vol. 20, No. 10, 1982, pp. 1426–1431.

[3]Takahashi, M., and Hayashi, A. K., "Numerical Study on Mixing and Combustion of Injecting Hydrogen Jet in a Supersonic Air Flow," AIAA Paper 91-0574, Jan. 1991.

[4]Shuen, J. S., and Yoon, S., "Numerical Study of Chemically Reacting Flows Using a Lower-Upper Symmetric Successive Overrelaxation Scheme," *AIAA Journal*, Vol. 27, No. 12, 1989, pp. 1752–1760.

[5]Speziale, C. G., Abid, R., and Anderson, E. C., "A Critical Evaluation of Two-Equation Models for Near Wall Turbulence," AIAA Paper 90-1481, June 1990.

[6]Yee, H. C., "A Class of High-Resolution Explicit and Implicit Shock-Capturing Methods," NASA TM-101088, Feb. 1989.

[7]Stull, D. R., and Prophet, H., "JANAF Thermochemical Tables," National Bureau of Standards NSRDS-NBS 37, 1971.

[8]Hirschfelder, J. O., Curtiss, C. F., and Bird, R. B., *Molecular Theory of Gases and Liquids*, John Wiley, New York, 1954.

[9]Wilke, C. R., "A Viscosity Equation for Gas Mixtures," *Journal of Chemistry and Physics*, Vol. 18, No. 4, 1950, pp. 517–519.

[10]Berman, H. A., Anderson, J. D., and Drummond, J. P., "Supersonic Flow Over a Rearward Facing Step with Transverse Nonreacting Hydrogen Injection," *AIAA Journal*, Vol. 21, No. 12, 1983, pp. 1701–1713.

[11]Rosner, D. E., *Transport Processes in Chemically Reacting Flow Systems*, Butterworths, Boston, 1986.

[12]Grasso, F., and Falconi, D., "On High Speed Turbulence Modeling of Shock-Wave Boundary-Layer Interaction," *AIAA Journal*, Vol. 31, No. 7, 1993, pp. 1199–1206.

[13]Abid, R., Speziale, C. G., and Thangam, S., "Application of a New k-τ Model to Near Wall Turbulent Flows," AIAA Paper 91-0614, Jan. 1991.

[14]Hanjalic, K., and Launder, B. E., "Contribution Towards a Reynolds Stress Closure for Low-Reynolds-Number Turbulence," *Journal of Fluid Mechanics*, Vol. 74, 1976, pp. 593–610.

[15]Roe, P. L., "Approximate Riemann Solvers, Parameter Vectors, and Difference Schemes," *Journal of Computational Physics*, Vol. 43, No. 2, 1981, pp. 357–372.

[16]Steger, J. L., and Warming, R. F., "Flux Vector Splitting of Inviscid Gasdynamics with Application to Finite Difference Methods," *Journal of Computational Physics*, Vol. 40, No. 2, 1981, pp. 263–293.

[17]Van Leer, B., "Flux-Vector Splitting for the Euler Equations," Institute for Computer Application in Science and Engineering, ICASE Rept. 82-30, Hampton, VA Sept. 1982.

[18]Liou, M. S., Van Leer, B., and Shuen, J. S., "Splitting of Inviscid Fluxes for Real Gases," *Journal of Computational Physics*, Vol. 87, No. 1, 1990, pp. 1–24.

[19]Liu, Y., and Vinokur, M., "Upwind Algorithms for General Thermo-Chemical Nonequilibrium Flows," AIAA Paper 89-0201, Jan. 1989.

[20]Grasso, F., and Bellucci, V., "Modeling of Hypersonic Nonequilibrium Flows," *Advances in Hypersonics*, edited by J. Bertin, J. Periaux, and J. Ballmann, Birkhauser, Boston, MA, Vol. 2, 1992, pp. 128–175.

[21]Zukoski, E. E., and Spaid, F. W., "Secondary Injection of Gases into a Supersonic Flow," *AIAA Journal*, Vol. 2, No. 10, 1964, pp. 1689–1696.

[22]Aso, S., Okuyama, S., Kawai, M., and Ando, Y., "Experimental Study on Mixing Phenomena in Supersonic Flows with Slot Injection," AIAA Paper 91-0016, Jan. 1991.